

Hydration and Ordering of Lamellar Block Copolymer Films under Controlled Water Vapor

Yohei Kamata,^{*,†,‡} Andrew J. Parnell,[‡] Philipp Gutfreund,[§] Maximilian W. A. Skoda,^{||} Andrew J. C. Dennison,^{§,⊥} Robert Barker,[§] Shaomin Mai,[#] Jonathan R. Howse,[&] Anthony J. Ryan,[#] Naoya Torikai,^{,@} Masami Kawaguchi,[@] and Richard A. L. Jones[‡]

[†]Kuraray Co., Ltd., 2045-1 Sakazu Kurashiki, Okayama 710-0801, Japan

[‡]Department of Physics and Astronomy, The University of Sheffield, Hicks Building, Hounsfield Road, Sheffield S3 7RH, United Kingdom

[§]Institut Laue-Langevin, 38042 Grenoble, Cedex 9, France

^{||}ISIS, STFC Rutherford-Appleton Laboratory, Harwell Science and Innovation Campus, Didcot OX11 0QX, United Kingdom

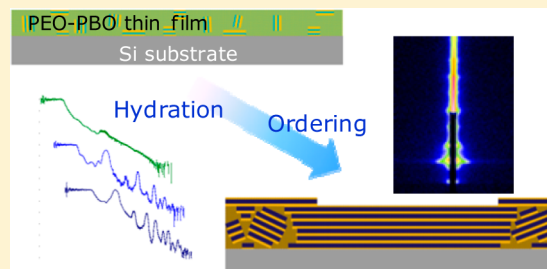
[⊥]Department of Physics and Astronomy, Uppsala University, Box 516, 751 20 Uppsala, Sweden

[#]Department of Chemistry, The University of Sheffield, Brook Hill, Sheffield S3 7HF, United Kingdom

[&]Department of Chemical and Biological Engineering, The University of Sheffield, Sir Robert Hadfield Building, Mappin Street, Sheffield S1 3JD, United Kingdom

[@]Department of Chemistry for Materials, Graduate School of Engineering, Mie University, 1577 Kurimamachiya, Tsu, Mie 514-8507, Japan

ABSTRACT: Amphiphilic block copolymers within a range of volume fraction spontaneously form vesicles in aqueous solution, where a water core is enclosed by a polymer bilayer. Thin-film rehydration is a method used to produce vesicles routinely; a thin film is immersed in water, the film swells, and vesicles are formed which bleb off from the film surface. We have studied the early stages of hydration for PEO–PBO block copolymer thin films under controlled water vapor conditions to understand this formation mechanism and so enable more efficient ways to encapsulate molecules using this method. Neutron and X-ray measurements show that the initial film exhibits weakly ordered structure with isotropic parallel and vertical orientation; the films initially swell and maintain the same orientation. At a critical point the layer swells rapidly and makes highly ordered lamellae structure at the same time. The lamellae are almost exclusively oriented parallel to the substrate and swell with increasing water absorption.



1. INTRODUCTION

Lipid molecules were among the first primitive biological containers on the primordial earth; they provided compartments that enabled complexity and specific cellular function in biological systems, all of which are essential for the evolution of life. It has been speculated that early life began in this environment. In this conjecture lipid-like molecules were present near hot rocky pools. Shallow fresh water pools would fill with water and over time the water would evaporate. Numerous drying and rehydration cycles would have resulted in the production of highly ordered layered lamellar nanostructures from the arrangement of amphiphilic lipids. When rehydrated these hierarchical structures would spontaneously self-assemble into micelles and vesicles. The repetition of wet and dry cycles would have concentrated amino acids and other small molecules; these would then be incorporated within the aqueous core of the liposomes as well as the hydrophobic membranes. These membrane bound structures were the beginning of cellular based life.

Modern cell biology routinely uses encapsulation processes to package a payload and transport it to a location where the payload can then be used. Cell biology works under confinement and not in a large test tube; partitioning of components is important to exclude certain molecules; corralling or enclosing molecules together is also vital to cellular function. Currently our ability to emulate this biological packaging process is poor, and if we are able to overcome some of these failings we will be able to fully develop a *Synthetic Biology* toolkit essential for this nascent field. Encapsulation technologies at present rely on forming a lipid vesicle and then extruding it in a solution containing the target molecule that is to be encapsulated. Only a small fraction is encapsulated in this process. Synthetic polymer based liposomes (polymersomes) are one possible way in which we can artificially contain a molecule of interest that is

Received: July 15, 2014

Revised: November 18, 2014

Published: December 12, 2014

protected from its surrounding environment. Polymersomes are vesicles composed of amphiphilic copolymers and have a number of advantages compared to naturally derived biobased liposomes in particular: their diverse chemistry, tunable membrane permeability, stability under high shear, variable adhesion, and ability to store hydrophobic and hydrophilic molecules. Also, they can have stealth-like properties, making them able to circulate in the body for a long time. The problem currently is the very low efficiency with which a particular molecule is sequestered inside. This is because of the complex structural formation pathway in going from individual isolated amphiphilic molecules into vesicle aggregates. This is first by the formation of micelles, then rod-like micelles, and subsequently isolated lamellar sheets. Vesicles then bud off the sheets in a blebbing or budding-off process. Therefore, and importantly, the vesicles formation route means that they do not act like Pac-Man and enclose a volume of solution; instead, the vesicle water core is filled with water, which has diffused through the vesicle membrane.

Polymer vesicles¹ do have potential as molecular delivery systems, as they self-assemble and can be easily tailored in size.² The thin film rehydration³ method has higher encapsulation efficiency than other preparation methods, as the block copolymer can be mixed with a molecule prior to vesicle formation.⁴ Other methods such as solvent switching lead to low levels of encapsulation due to the kinetic formation pathway.⁵

In this work we have studied the hydration and ordering of thin films under controlled water vapor flow conditions to establish the very early stages before the complex processes. The materials used in this work—ethylene oxide–butylene

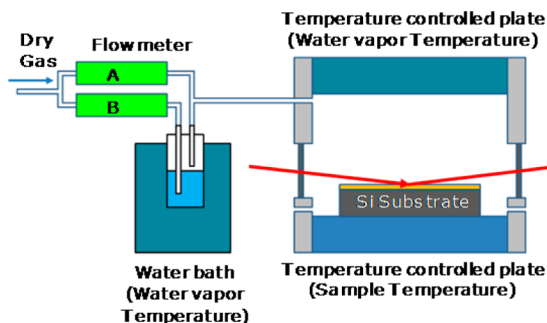


Figure 1. Schematic representation of the water vapor flow chamber used for the neutron reflectivity experiments. The other chambers for AFM, ellipsometry, and GISAXS had similar water vapor flow controlling systems.

oxide (EB) diblocks—have well characterized equilibrium phase diagrams in both the melt⁶ and the semicrystalline state.⁷ The exact same EB diblock copolymer used in this study has been comprehensively studied in the *later stages* of vesicle formation.⁸ In the later stages of vesicle formation the vesicle forming polymer has already formed a lamellar gel, as determined by small-angle X-ray scattering.⁹ In this work we also wanted to examine how we can solvent anneal these vesicle forming polymers to get them in a state of readiness for vesicle formation and so improve their formation rate.

In thin films, the influence of surfaces and interfaces on the morphology is important.^{10,11} An early study of poly(ethylene oxide)–polybutadiene copolymers showed dewetted structures on hydrophobic substrates that formed terraces with a single crystal of PEO running throughout each isolated structure.¹² These were connected by screw dislocations in the lamellae, pointing to increased complexity in these types of materials compared to simple diblock copolymer melts. Thin film morphologies

of symmetric (i.e., 50:50) semicrystalline EB diblock copolymers have been extensively studied, and the effects of chain length, annealing, and substrate surface energy have been examined. For low molar mass block copolymers of comparable molecular weight to the ones used here, after annealing the morphology consists of lamellae oriented parallel to the substrate surface.¹³ This preferred orientation may be controlled by changing the functionalization of the substrate surface.¹⁴ In the current study, we follow in detail the way an initially disordered thin film orders on exposure to water vapor *in situ* using an environmental chamber (Figure 1).

2. EXPERIMENTAL SECTION

Materials. The block copolymer PEO₁₁₅PBO₁₀₃ ($M_w = 12\,500$) was prepared by sequential anionic polymerization using high vacuum

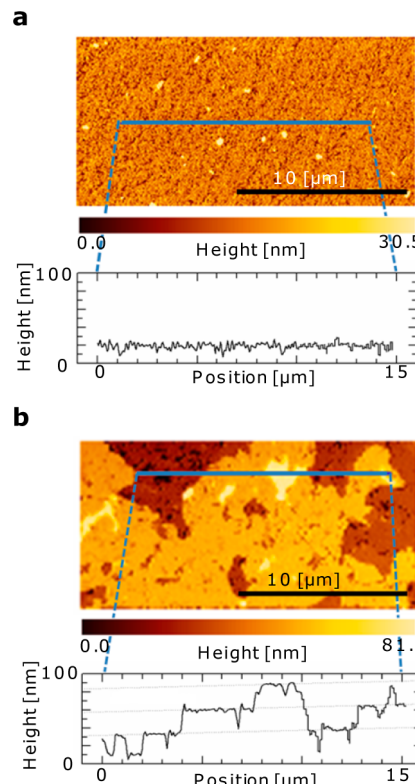


Figure 2. *In situ* measurements of AFM: (a) AFM height image and cross-sectional height image of the initial dry film surface; (b) AFM height image and cross-sectional height image of the film surface that was annealed with water vapor flow for 150 min.

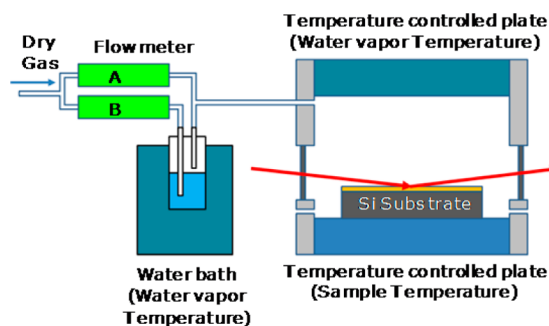


Figure 3. Time-dependent change of the block copolymer films during the hydration in different water vapor flow temperature conditions, measured using ellipsometry.

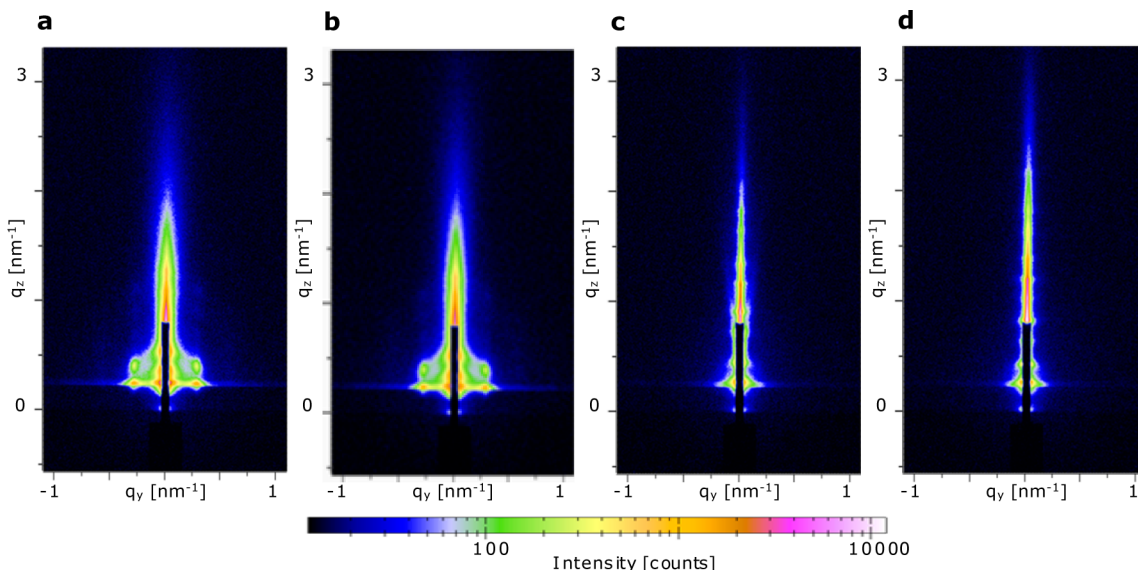


Figure 4. *In situ* GISAXS measurements: (a) initial dry film; (b) after 30 min water vapor annealing; (c) after 34 min water vapor annealing; (d) after 66 min water vapor annealing.

techniques.¹⁵ The molecular weight and volume fraction were estimated by gel permeation chromatography and ^{13}C NMR. The volume fraction of PEO (ϕ_E) units was 0.37. The melt morphology at 70 °C for this polymer is hexagonal cylinders of PEO in a matrix of PBO.

Sample Preparation. Silicon substrates of 1 mm thickness 20 × 20 mm² were used for grazing-incidence small-angle X-ray scattering (GISAXS), ellipsometry, and atomic force microscopy (AFM) measurements. For the neutron reflectivity (NR) experiments 100 mm diameter, 10 mm thickness silicon substrates were used to provide a large sample area, which enabled the swelling kinetics to be measured effectively using NR. The silicon substrates were oxygen plasma cleaned prior to spin coating with monocarboxy-terminated polystyrene (PS-COOH, $M_w = 13\,000$, Scientific Polymer Products, Inc.). A PS-COOH toluene solution (5 wt %) was spin-cast onto the native oxide surface of the silicon substrates to stabilize the spin-coated block copolymer and prevented dewetting. The substrates were then thermally annealed at 150 °C under vacuum conditions for 4 days. Ungrafted PS-COOH polymer was removed by washing the substrates with toluene. The thickness of the grafted PS layer on the substrates was less than 3 nm, as measured by NR and ellipsometry. Thin films of PEO₁₁₅PBO₁₀₃ were prepared by spin-coating a solution of the block polymer in chloroform (0.75 wt %) at 3000 rpm onto the polystyrene (PS-COOH)-modified silicon substrates. The initial thickness of the PEO₁₁₅PBO₁₀₃ layer was controlled within a range of 70–125 nm. Neutron reflectivity shows that the PBO layer was preferentially formed as the first layer on the hydrophobic polystyrene modified substrate.

Water Vapor Flow Chamber. AFM, GISAXS, ellipsometry, and NR were performed in a water vapor flow chamber to allow control of the water temperature and moisture content; this is shown schematically in Figure 1. The amount of water vapor in the flow gas was controlled by adjustment of the water vapor temperature and flow rates of dry gas and water infused gas. The sample was maintained at a constant temperature to avoid thermal expansion. The thickness change is defined as a ratio of the thickness change from its initial dry thickness to its total thickness. Sample temperature was fixed during the measurement, so these results may not include thermal expansion. Therefore, this thickness change is considered to be almost equal to the water volume fraction in a thin film sample. For these experimental conditions, the higher water temperature flow gas included a higher concentration of water. Optical ports (7 mm diameter) were used as windows for the ellipsometry measurements, and 0.1 mm thick double-polished silicon wafers were used as windows for the NR experiments. Kapton film of 7.5 μm thickness was used as windows for

the GISAXS measurements. It should be mentioned that the chambers used for each measurement had different volumes and were made of different materials, so the swelling behavior time scales from each measurements could not be compared directly.

Atomic Force Microscopy. The atomic force microscopy measurements of the thin film surface were carried out using a SII NanoTechnology Inc. E-sweep operated in tapping mode. The AFM tips were SII NanoTechnology Inc. SI-DF3, and these spring constants were around 1.5 N/m. Dry air was used for the flow gas and H₂O infused gas. The sample was dried with a flow of dry air (flow 1.0 L/min) for over 2 h before the water vapor annealing started. In the water vapor annealing measurements, the flow rate of dry air was 0.15 L/min and the flow rate of H₂O infused air was 1.85 L/min. The water vapor temperature and sample temperature were fixed at 22 °C. Multiple sample areas were measured to minimize any potential sample damage from the AFM tapping measurements.

Ellipsometry. A spectroscopic ellipsometer (J.A. Woollam Co. M2000v) was used for the *in situ* ellipsometry measurements. Dynamic reflection data (ψ and Δ) were recorded every 10 s over a wavelength range of 375–1000 nm. The PEO₁₁₅PBO₁₀₃ thin films were regarded as a homogeneous layer during the water vapor hydration process, permitting us to determine film thickness using a Cauchy model over the measurement wavelength range.¹⁶ Dry nitrogen was used for the flow gas and H₂O infused gas. Samples were dried with dry nitrogen flow (1.0 L/min) for over 2 h before the water vapor annealing started. The flow rate of dry nitrogen was 0.0 L/min, and the flow rate of H₂O infused nitrogen was 1.0 L/min in the water vapor annealing measurements. The sample temperature was kept constant at 20 °C.

Grazing Incidence Small-Angle X-ray Scattering. Grazing incidence small-angle X-ray scattering (GISAXS)¹⁷ was performed to resolve the in-plane and out-of-plane structure of the thin polymer film during hydration/dehydration. The measurements were performed on the beamline BL03XU at SPring-8 (Japan) with 0.1 nm wavelength X-rays.¹⁸ The incident angle was fixed as 1.2°. An imaging plate detector was used for detection of the scattered X-rays. Dry helium was used as the flow gas to reduce background scattering. The sample was dried with dry helium flow (1.0 L/min) for over 1 h before the water vapor annealing started. The flow rate of dry helium was 0.0 L/min, and the flow rate of H₂O infused gas was 1.0 L/min in the *in situ* measurement. The water vapor temperature and sample temperature were fixed at 20 °C.

Neutron Reflectivity. Neutron reflectivity (NR)¹⁷ was performed to resolve the out-of-plane structure of the thin polymer film during hydration/dehydration with a particular emphasis on the (heavy) water distribution in the layer due to the high sensitivity of neutrons to

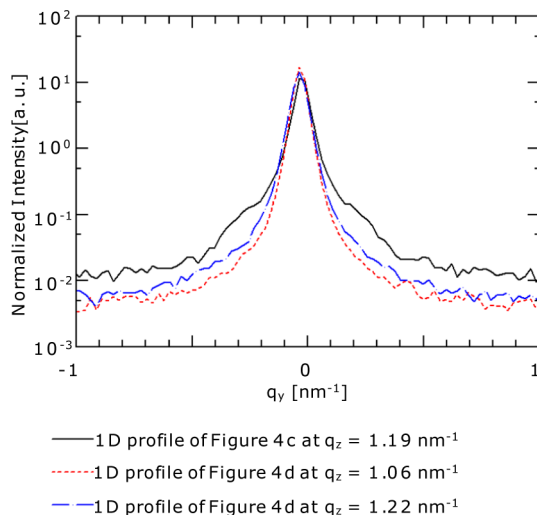


Figure 5. One-dimensional scattering profiles of the in-plane momentum transfer of the GISAXS pattern in Figure 4c ($q_z = 1.19 \text{ nm}^{-1}$), Figure 4d ($q_z = 1.06 \text{ nm}^{-1}$), and Figure 4d ($q_z = 1.22 \text{ nm}^{-1}$).

deuterium in this case. Two different experimental conditions were chosen to obtain NR data over a wide range of water absorption and also to capture the fast swelling kinetics. The time-of-flight mode neutron reflectivity measurements were performed on D17¹⁹ at the ILL with neutron wavelengths ranging from 2 to 25 Å and on INTER²⁰ at ISIS with neutron wavelengths ranging from 1.5 to 14 Å. Dry nitrogen was used for the flow gas. D₂O was used for water vapor gas to reduce background scattering (the incoherent background from H₂O would have limited the reflectivity dynamic range) and most importantly to obtain strong scattering contrast between the two polymer components. The samples were dried with dry nitrogen flow (1.0 L/min) for over 2 h before the water vapor annealing started. The flow rate of dry nitrogen was 0.0 L/min, and the flow rate of D₂O infused gas was 1.0 L/min in the water vapor annealing measurements. The sample temperature was fixed at 20 °C. The water vapor temperature of the

experiments on D17 was stepwise increased as shown in Figure 6a in order to cover a wide water absorption range. The water temperature of the measurements on INTER was fixed as 18 °C to see the fast early stage kinetics. Neutron reflectivity data were collected every 5 min repeatedly on INTER while on D17 they were accumulated between the two solid lines in Figure 6a.

Analysis of the Drying Process after the Hydration and Ordering. Neutron reflectivity measurements were also performed during the drying process after the 1400 min of water vapor annealing measurements on D17. The flow rate of dry nitrogen was changed to 1.0 L/min, and the flow rate of D₂O infused gas was changed to 0.0 L/min at 1400 min from the water vapor annealing start point. The sample temperature was kept at 20 °C, and the dry nitrogen gas temperature was fixed at 25 °C. Neutron reflectivity data were collected every minute repeatedly for 190 min and then summed over 10 min. The static GISAXS measurement was performed with the dried sample after the hydration on BL03XU at SPring-8 in a vacuum condition. The X-ray wavelength was 0.1 nm and the incident angle was 1.2°.

3. RESULTS AND DISCUSSION

The thin film samples have a smooth surface (Figure 2a) prior to vapor annealing. The root-mean-squared roughness parameter (R_{RMS}) of the dry thin film surface as determined from AFM was 4.0 nm. After 150 min water vapor annealing, AFM reveals a terraced surface morphology. Four different terrace surfaces were observed from above the surface, and the surfaces of the top, second, third, and bottom are depicted as yellow, orange, brown, and dark brown colors, respectively, in Figure 2b. The thickness values of the top and second terrace layer are 27.8 ± 3.3 and 24.8 ± 4.1 nm, respectively. These thicknesses are similar to the bulk value of 23 nm for the nonequilibrated lamellar spacing (Figure 2b).²¹ The time dependence of the swelling of the films as they take up water vapor is revealed by ellipsometry in Figure 3. For water temperatures of 17 °C there was no appreciable swelling; higher water temperatures lead to faster swelling and a larger final swelling ratio. The kinetics of

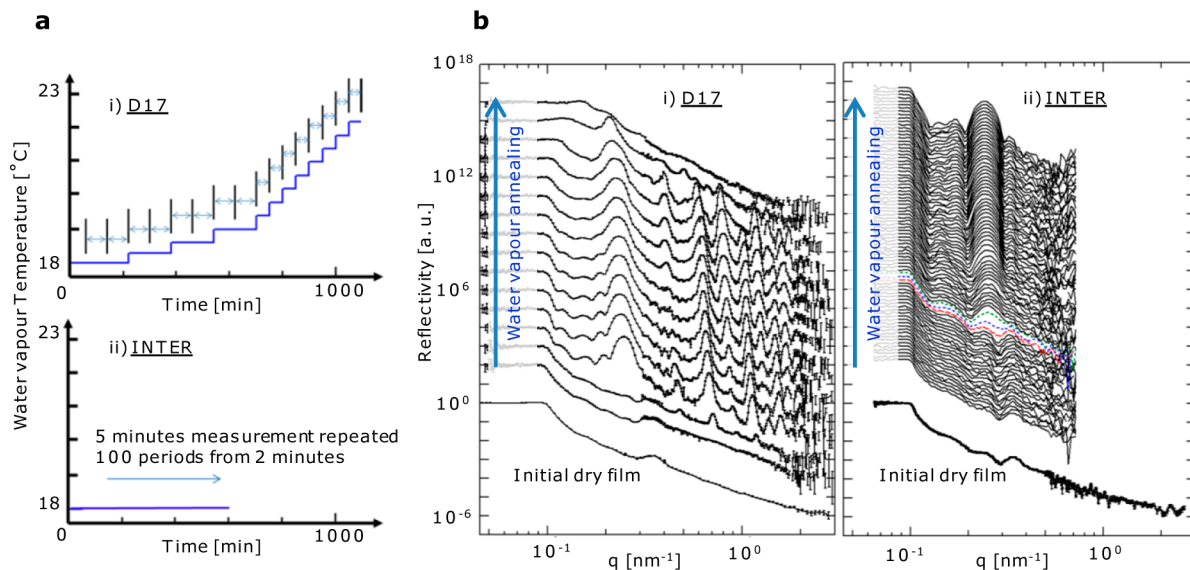


Figure 6. *In situ* neutron reflectivity measurements. (a) The water vapor temperature conditions for the neutron reflectivity measurements on D17 at the ILL (i)²² and on INTER at ISIS (ii). The water vapor temperature is plotted against the water vapor annealing time. Neutron reflectivity profiles were accumulated in between each separated lines, shown by a double-headed arrow on D17 and in every 5 min on INTER. (b) Kinetic neutron reflectivity results measured using the reflectometers D17 at the ILL and INTER at the ISIS: (i) D17 measurements; (ii) INTER measurements; the data for both plots are offset to aid clarity. The data set at 10^0 is the initial reflectivity data for the dry thin film; in the vertical direction is a time sequence of the profiles obtained during the water vapor annealing, which have been offset for clarity.

swelling displays initial slow uptake of water until the thickness is 2.5–5% higher than its initial value; this induction stage is followed by very rapid swelling and then a final asymptotic approach to an equilibrium degree of swelling.

The GISAXS data (Figure 4) for the initial dry film contains diffraction spots for the in-plane direction and out-of-plane directions; the initial spin-coated film has weakly ordered, phase-separated structures that are oriented vertically and horizontally. The peak position, q^* , of the in-plane orientation is 0.281 nm^{-1} , and its d spacing ($d = 2\pi/q^*$) is 22.4 nm. The pattern and d spacing remain little changed during the initial phase of water uptake, but after 34 min exposure, the diffraction spots from the in-plane direction disappeared, and strong diffraction spots with higher orders in the out-of-plane direction appeared. We conclude that at this point the film abruptly switches lamellar orientation where the lamellae are exclusively parallel to the substrate interface. After this structural change, the diffraction spots in the out-of-plane direction shifted to lower q region, and the widths of the spots became narrower with water vapor annealing (Figure 5). These may indicate that the lamellae kept swelling and orientating parallel after the structural change point.

Figures 6b-i²³ and 6-ii are the *in situ* neutron reflectivity results for different time scales of vapor exposure. The reflectivity profiles at 10^0 (lowest data set) are the data for the initial dry thin films before hydration. They show weak, broad peaks for the initial dry films at a q value of 0.34 nm^{-1} ($d = 18.5 \text{ nm}$). The next data set in the vertical direction begins a sequence of neutron reflectivity measurements obtained *in situ* during water vapor annealing. The fourth profile in the sequence of Figure 6b-i—taken after 220–300 min—shows a series of strong diffraction peaks, with many higher orders. The peak positions shift to lower q with further exposure. Toward the end of the process, the critical edge moves to higher q due to the severely water (D_2O) saturated conditions causing condensation on the film surface; here macroscopic surface water droplets cause diffuse scattering. Figure 6b-ii shows a similar sequence with finer time resolution for the earlier stages of the process. The structural rearrangement transition to exclusive out-of-plane ordering, which is also seen in the GISAXS measurements, is bracketed by the two dotted line profiles, showing that it is completed in less than 15 min.

The reflectivity at early times was modeled with a single laterally homogeneous layer with weakly ordered domains; at later times a linear combination of multilamellar layers was used, corresponding to highly ordered lamellar structures almost entirely oriented parallel to the substrate (Figure 7a–c). To fit such lamellar structures, a linear combination model was used which included two distinct lamellar layer models with different numbers of layers (for example, 5 and 6 layers were used in Figure 7b). The film may also have many nonequilibrium lamellar layer structures throughout the film thickness. However, in this analysis, such complicated inner structures were excluded, and a single homogeneous layer model was used to fit the data and obtain an average for the total layer thickness and an effective average scattering length density of the film. In the fitting procedure, the calculated water volumes from the thickness change and the scattering length density profile were kept consistent with each other. The scattering length density values of PEO, PBO, and D_2O were calculated to be 6.45×10^{-7} , 2.09×10^{-7} , and $6.33 \times 10^{-6} \text{ \AA}^{-2}$, respectively (calculated using the NIST database). The densities of PEO and PBO were estimated as 1.14 and 1.01 g/cm^3 , respectively, by the Van

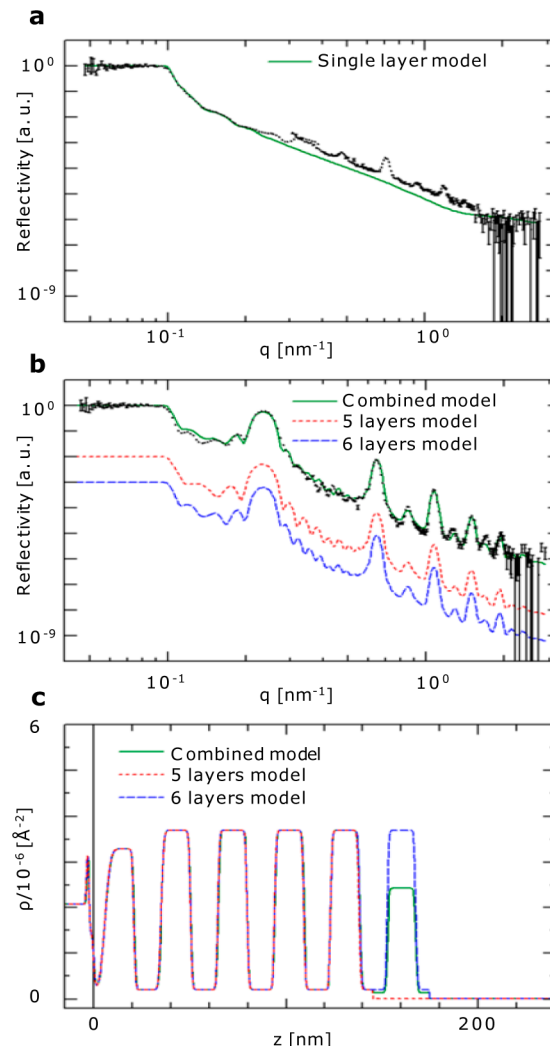


Figure 7. (a) Neutron reflectivity profile of a single layer model. (b) Neutron reflectivity data fitted to a lamellar model with 5 and 6 layers along with a linear mixed combination of the two models. (c) Scattering length density profiles of (b).

Krevelen's group additive method.²³ The package Motofit²⁴ was used for fitting the reflectivity data. The scattering length density of the top PEO layer has a lower value than the other buried PEO layers. This does not mean the top PEO layer has lower water absorption but is a result of summing two lamellar layers models with different number of layers. Lower scattering length density (SLD) corresponds to PBO layers, and higher SLD corresponds to water (D_2O) swollen PEO layers in Figure 7c. The errors of the total thickness and the SLD value with the single layer model were estimated smaller than $\pm 1.4\%$ and $\pm 7.4\%$, respectively. The errors of the PBO layer thickness, PEO layer thickness, and the SLD value of the PEO layer with the multilayers model were estimated smaller than $\pm 2.4\%$, $\pm 2.0\%$, and $\pm 7.3\%$, respectively.

Figure 8 shows the evolution of the scattering length density profiles during the hydration process for two different time scales. Film thickness and scattering length density increase with water absorption, and periodic lamellar structure appears after the structural transition point.

Figure 9 shows the volume of absorbed water and the thickness changes of the PEO–PBO bilayer and the PBO layer with water vapor exposure time. The volume of absorbed water

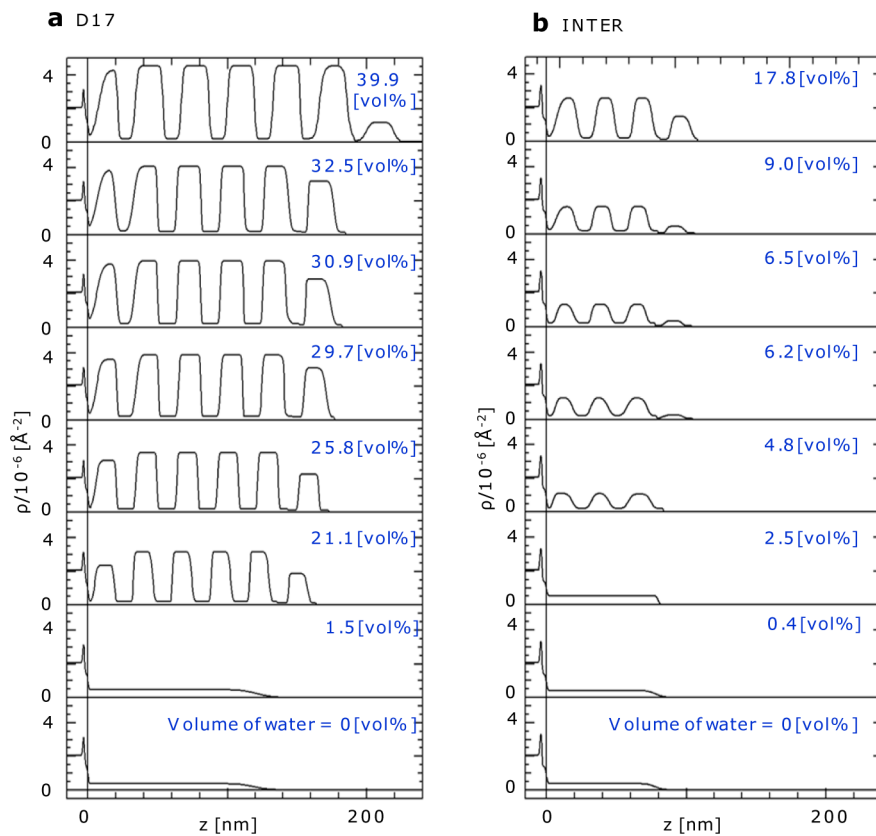


Figure 8. Evolution of scattering length density profiles during the hydration process: (a) from the D17 data; (b) from the INTER data. The horizontal axis z means film depth, and the origin position of z is the interface between modified polystyrene layer and the $\text{PEO}_{115}\text{PBO}_{103}$ film layer. The initial film thicknesses for the D17 sample and the INTER sample were 119.2 and 77.8 nm, respectively.

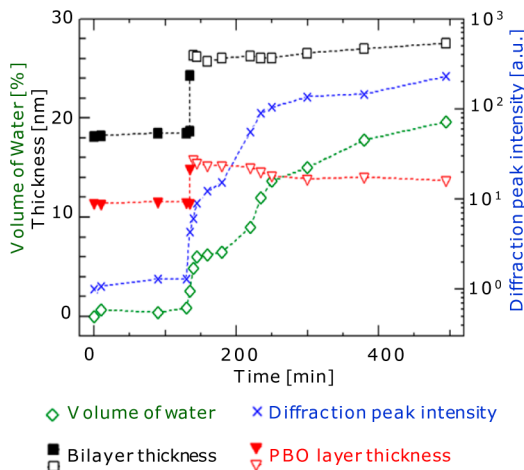


Figure 9. Structural changes during the rehydration process. The $\text{PEO}-\text{PBO}$ bilayer thickness, PBO single layer thickness, the first diffraction peak intensity, and also the volume of the absorbed water as a function of the water vapor annealing time from the INTER results. The thicknesses of the bilayer and the PBO layer are indicated by filled symbols, these values were evaluated from the initial weak diffraction peak position, and those indicated by open symbols were evaluated using the scattering length density profiles.

increased rapidly after it reached 2.5 vol % water, in agreement with the ellipsometry swelling results. The intensity of the first diffraction peak and the thickness of the $\text{PEO}-\text{PBO}$ bilayer and PBO layer also increased rapidly after the volume of absorbed water reached 2.5%.

To understand the mechanism behind the structural change from the neutron reflectivity results, in Figure 10 we plot the thickness changes of the $\text{PEO}-\text{PBO}$ bilayer and the PBO layer. We also plot the first diffraction peak intensity against the volume of absorbed water in Figure 10. The initial bilayer thickness was 18.2 nm, rather less than the 22.4 nm evaluated using GISAXS. This may indicate that the film was extended in the horizontal direction and fixed its structure during the rapid nonequilibrium spin-coating process. After the structural transition, the bilayer thickness gradually increased with water absorption, while the PBO layer thickness slightly decreased. To maintain the overall mass of the hydrophobic PBO layer, its thickness decrease must be accompanied by a swelling in the horizontal direction, i.e., parallel to the surface. As the lamella area is fixed by the chemical bonds between PBO-PEO, the PEO layer must be swollen in the horizontal direction as well.

The diffraction peak intensity also increased abruptly in the same range from 2.5% to 5% in water volume content followed by a further rapid increase up to 10% in water volume. This suggests that lamellae could be gradually oriented parallel to the substrate in this water volume range. After that, the intensity increased according to the water absorption because of enhancement of the PEO layer scattering length density with D_2O .

The experimental values for bilayer thickness were compared with self-consistent field theory (SCFT) calculations using the program “OCTA”.²⁵ The solid and broken lines in Figure 10 are the calculated bilayer and PBO layer thicknesses supposing a bulk, equilibrium system at the measured water concentration. At higher water volume fractions there is a good correspondence between data and theory for both the bilayer and PBO

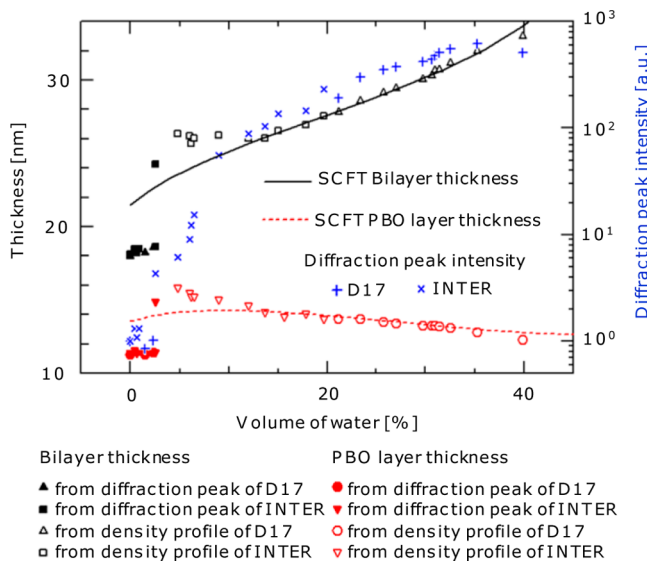


Figure 10. Structural changes during the rehydration process. The PEO–PBO bilayer thickness, PBO single layer thickness, and also the first diffraction peak intensity as a function of the volume of absorbed water. The bilayer thickness from the D17 results is indicated by triangle symbols and those of INTER by square symbols. The PBO layer thickness from the D17 results are displayed by circle symbols, while those of INTER are indicated by inverted triangle symbols. The thickness of the bilayer and the PBO layer are indicated by filled symbols, evaluated using the initial weak diffraction peak position, and those indicated by open symbols were evaluated using the scattering length density profiles. The diffraction peak intensity is indicated by plus signs for the D17 results and by \times symbols for INTER results. Solid line and broken line show calculation of the bilayer thickness and the PBO layer thickness results of a bulk lamella system of A(PEO model)–B(PBO model) diblock copolymer and C(water model) homopolymer by SCFT calculations with $N_{\text{block A}} = 37$, $N_{\text{block B}} = 63$, and $N_{\text{block C}} = 3$. Interaction parameters $\chi_{AB} = 0.4$, $\chi_{AC} = 0.0$, and $\chi_{BC} = 3.0$. Calculated structural sizes were scaled by multiplying the same constant value.

layer thicknesses, implying the film can equilibrate on a faster time scale than water diffusion. However, below 2.5% in the water volume fraction, both the layer thicknesses are much lower than the SCFT calculations, showing that the blocks are unable to rearrange quickly enough to stay in local equilibrium with the increasing water content. After the abrupt structural change, the bilayer and PBO layer thickness are slightly higher than the SCFT calculation results. During the onset of rapid structural change, the film formed ordered lamellar structures which swell and expand rapidly. Such a rapid deformation of the lamellar structure may induce internal stress and cause the lamellar grains to compress each other. Such internal stress may increase the thickness of the horizontally ordered lamellae.

From all the results, the structural model of the hydration and ordering for PEO₁₁₅PBO₁₀₃ thin films during water vapor annealing is shown in Figure 11. The initial dry spin-coated film has some weak phase-separated structures that are oriented parallel and vertical to the substrate. This does not change until the 2.5% water absorption point is reached. When the water volume exceeds about 2.5%, the film swells rapidly and forms an ordered lamellar structure. The lamellae are then gradually oriented parallel to the substrate until around 10% water content, after which the lamellar thickness increases with water absorption. It is still not clear what determines such rapid structural changes. One possibility is that the PEO block forms

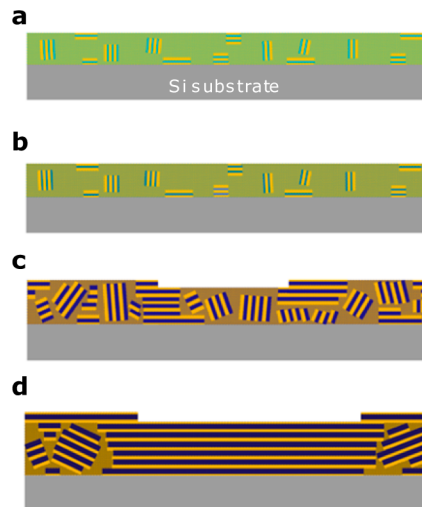


Figure 11. Drawing of the proposed structural model during the rehydration process: (a) the initial dry film; (b) with water absorption volume up to 2.5%; (c) after the rapid structural change region; (d) above 10% in the water absorption volume.

crystalline domains in the initial spin-coated film, which remain and pin the structure up to this specific amount of water absorption. Another possibility is that the PEO phase regions are isolated in the initial film, preventing water penetration into the film.

We have also examined the drying process after the film was hydrated and ordered (Figure 12a).²² There is a diffraction peak with diffuse scattering in the reflectivity profile after extended water vapor annealing. The peak position is 0.163 nm⁻¹, and the corresponding *d*-spacing is 38.5 nm. It is difficult to be definitive about the structural origin of this peak. One possibility is that this peak arises from the lamellae unbinding length scale, which does not change during the total changes in the absorbed water content due to the preferential water absorption into one layer. Another possibility is that the stacked lamella changes to a different ordered structure with increased water absorption. In the bulk state, this block copolymer forms a sponge phase structure at higher water volume fractions.⁶ But, given that the diffraction peak observed in the thin film is substantially larger than that expected for the sponge phase, this seems a less likely explanation.

During the drying process the strong diffraction peak of the stacked lamellae appeared, and the initial “wet” peak shifted to higher *q*. The intensity of the stacked lamellae diffraction peak gradually decreased throughout the drying process and finally disappeared. To see the structural change in the sample plane as well, a static GISAXS measurement was also performed on the hydrated and ordered dried film after a long hydration period. Figures 12b and 12c show the GISAXS pattern and the integration for the in-plane momentum transfer direction. There were two peaks in the in-plane direction. The diffraction peak in the in-plane direction at position 0.292 nm⁻¹ (*d*-spacing 21.5 nm) with its second order at 0.593 nm⁻¹ shows that the nanostructure of the film changed dramatically after the film dried. We conclude that the GISAXS pattern for the dry film is due to crystallization of the PEO, with the crystal stems oriented perpendicular to the lamellae. Because of the restriction of the block copolymer nanostructure, the vertically confined PEO has crystallized between the confining walls of the amorphous PBO, with a characteristic in-plane length scale. An earlier SAXS study has previously identified this same identical behavior

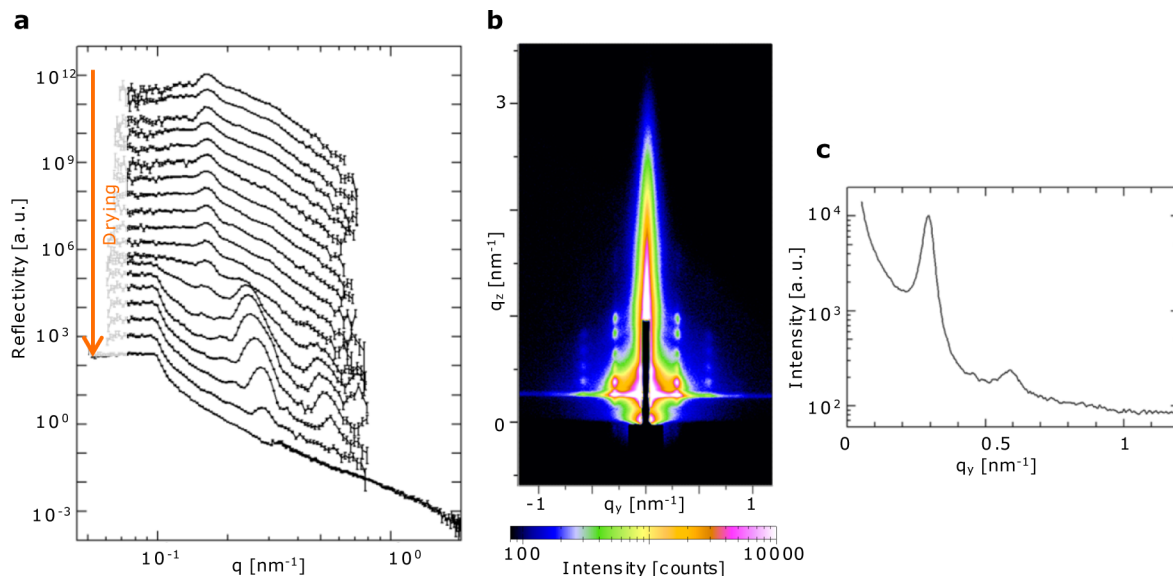


Figure 12. Structural changes of the drying process. (a) *In situ* neutron reflectivity results measured using D17 at the ILL in the drying process after 1400 min water vapor annealing.²² From the top to the bottom profiles measured at 10, 20, 30, 40, 50, 60, 70, 80, 90, 100, 110, 120, 130, 140, 150, 160, 170, 180, and 190 min after the drying gas flow started. The water vapor flow was stopped after 1400 min from the start of water vapor annealing, and then a flow of dry nitrogen flow commenced. (b) Two-dimensional scattering pattern of the static GISAXS measurement of the dried sample after prolonged water vapor annealing. (c) One-dimensional scattering profile of the in-plane momentum transfer of the GISAXS pattern in (b).

for a similar semicrystalline block copolymer system of poly(ethylene)-poly(vinylcyclohexane). A simple Markov model was used to simulate the diffuse scattering within and between a linear positioning of poly(ethylene) crystallites.²⁶

4. CONCLUSION

In summary, the hydration and ordering of a vesicle forming PEO-PBO block copolymer thin film was investigated. *In situ* GISAXS and neutron reflectivity experiments showed that there is a fast structural transition in the hydration process, where the film swells rapidly and forms highly ordered lamellae exclusively oriented parallel to the substrate. The experimental results were complemented by self-consistent field theory calculations, which showed a good agreement after the fast reordering of the lamellae during swelling. *In situ* measurements during subsequent drying of the sample showed that the structural change is partly reversible. Solvent annealing may thus be a promising route to improve vesicle formation by effectively ordering the surface on a mesoscopic length scale.

AUTHOR INFORMATION

Corresponding Author

*E-mail: (Y.K.) yohei_kamata@kuraray.co.jp.

Notes

The authors declare no competing financial interest.

ACKNOWLEDGMENTS

A.J.P. was funded by the EPSRC under Grant EP/E046215/1 (Soft Nanotechnology). A.J.C.D. was funded by the Swedish Research Council (VR). We thank the ILL Neutron facility for time on D17 and the ISIS Neutron facility for time on INTER. We are grateful to the Polymer Subworkshop Group members of the Japan Association for the Chemical Innovation (JACI) and Dr. D. Martin A. Buzzo for valuable advice about SCFT calculations. We are grateful to Professor J. Patrick A. Fairclough for helpful discussions concerning our understanding of the GISAXS pattern for the dried sample. The GISAXS measurements

were carried out at the first hutch of SPring-8 BL03XU constructed by the Consortium of the Advanced Softmaterial Beamline (FSBL) (Proposal No. 2011B7256 and 2012A7207).

REFERENCES

- (1) Discher, D. E.; Eisenberg, A. Polymer vesicles. *Science* **2002**, *297* (5583), 967–973.
- (2) Howse, J. R.; Jones, R. A. L.; Battaglia, G.; Ducker, R. E.; Leggett, G. J.; Ryan, A. J. Templated formation of giant polymer vesicles with controlled size distributions. *Nat. Mater.* **2009**, *8* (6), 507–511.
- (3) Du, J.; O'Reilly, R. K. Advances and challenges in smart and functional polymer vesicles. *Soft Matter* **2009**, *5* (19), 3544–3561.
- (4) Parnell, A. J.; Tzokova, N.; Topham, P. D.; Adams, D. J.; Adams, S.; Fernyhough, C. M.; Ryan, A. J.; Jones, R. A. L. The efficiency of encapsulation within surface rehydrated polymersomes. *Faraday Discuss.* **2009**, *143* (0), 29–46.
- (5) (a) Adams, D. J.; Adams, S.; Atkins, D.; Butler, M. F.; Furzeland, S. Impact of mechanism of formation on encapsulation in block copolymer vesicles. *J. Controlled Release* **2008**, *128* (2), 165–170. (b) Blanazs, A.; Madsen, J.; Battaglia, G.; Ryan, A. J.; Armes, S. P. Mechanistic insights for block copolymer morphologies: How do worms form vesicles? *J. Am. Chem. Soc.* **2011**, *133* (41), 16581–16587.
- (6) Ryan, A. J.; Mai, S.-M.; Fairclough, J. P. A.; Hamley, I. W.; Booth, C. Ordered melts of block copolymers of ethylene oxide and 1,2-butylene oxide. *Phys. Chem. Chem. Phys.* **2001**, *3* (15), 2961–2971.
- (7) Xu, J.-T.; Fairclough, J. P. A.; Mai, S.-M.; Chaibundit, C.; Mingvanish, M.; Booth, C.; Ryan, A. J. Crystallization behavior of oxyethylene/oxybutylene diblock and triblock copolymers. *Polymer* **2003**, *44* (22), 6843–6850.
- (8) Battaglia, G.; Ryan, A. J. The evolution of vesicles from bulk lamellar gels. *Nat. Mater.* **2005**, *4* (11), 869–876.
- (9) Battaglia, G.; Ryan, A. J. Bilayers and interdigititation in block copolymer vesicles. *J. Am. Chem. Soc.* **2005**, *127* (24), 8757–8764.
- (10) (a) Albert, J. N. L.; Epps, T. H., III Self-assembly of block copolymer thin films. *Mater. Today* **2010**, *13* (6), 24–33. (b) Luo, M.; Epps, T. H. Directed block copolymer thin film self-assembly: Emerging trends in nanopattern fabrication. *Macromolecules* **2013**, *46* (19), 7567–7579.
- (11) Di, Z.; Posselt, D.; Smilgies, D.-M.; Li, R.; Rauscher, M.; Potemkin, I. I.; Papadakis, C. M. Stepwise swelling of a thin film of

lamellae-forming poly(styrene-*b*-butadiene) in cyclohexane vapor. *Macromolecules* **2012**, *45* (12), 5185–5195.

(12) Hong, S.; MacKnight, W. J.; Russell, T. P.; Gido, S. P. Orientationally registered crystals in thin film crystalline/amorphous block copolymers. *Macromolecules* **2001**, *34* (8), 2398–2399.

(13) Liang, G.-D.; Xu, J.-T.; Fan, Z.-Q.; Mai, S.-M.; Ryan, A. J. Thin film morphology of symmetric semicrystalline oxyethylene/oxybutylene diblock copolymers on silicon. *Macromolecules* **2006**, *39* (16), 5471–5478.

(14) (a) Liang, G.-D.; Xu, J.-T.; Fan, Z.-Q.; Mai, S.-M.; Ryan, A. J. Effect of substrate surface on dewetting behavior and chain orientation of semicrystalline block copolymer thin films. *J. Phys. Chem. B* **2006**, *110* (48), 24384–24389. (b) Liang, G.-D.; Xu, J.-T.; Fan, Z.-Q.; Mai, S.-M.; Ryan, A. J. Effect of substrate and molecular weight on the stability of thin films of semicrystalline block copolymers. *Langmuir* **2007**, *23* (7), 3673–3679. (c) Liang, G.-D.; Xu, J.-T.; Fan, Z.-Q.; Mai, S.-M.; Ryan, A. J. Morphology of semicrystalline oxyethylene/oxybutylene block copolymer thin films on mica. *Polymer* **2007**, *48* (24), 7201–7210.

(15) Hsieh, H. L.; Quirk, R. P. *Anionic Polymerization: Principles and Practical Applications*; CRC Press: Boca Raton, FL, 1996.

(16) Weir, M. P.; Heriot, S. Y.; Martin, S. J.; Parnell, A. J.; Holt, S. A.; Webster, J. R. P.; Jones, R. A. L. Voltage-induced swelling and deswelling of weak polybase brushes. *Langmuir* **2011**, *27* (17), 11000–11007.

(17) Daillant, J.; Gibaud, A. *X-ray and Neutron Reflectivity - Principles and Applications*; Springer: Heidelberg, 2009.

(18) (a) Masunaga, H.; Ogawa, H.; Takano, T.; Sasaki, S.; Goto, S.; Tanaka, T.; Seike, T.; Takahashi, S.; Takeshita, K.; Nariyama, N.; Ohashi, H.; Ohata, T.; Furukawa, Y.; Matsushita, T.; Ishizawa, Y.; Yagi, N.; Takata, M.; Kitamura, H.; Sakurai, K.; Tashiro, K.; Takahara, A.; Amemiya, Y.; Horie, K.; Takenaka, M.; Kanaya, T.; Jinmai, H.; Okuda, H.; Akiba, I.; Takahashi, I.; Yamamoto, K.; Hikosaka, M.; Sakurai, S.; Shinohara, Y.; Okada, A.; Sugihara, Y. Multipurpose soft-material SAXS/WAXS/GISAXS beamline at SPring-8. *Polym. J.* **2011**, *43* (5), 471–477. (b) Ogawa, H.; Masunaga, H.; Sasaki, S.; Goto, S.; Tanaka, T.; Seike, T.; Takahashi, S.; Takeshita, K.; Nariyama, N.; Ohashi, H.; Ohata, T.; Furukawa, Y.; Matsushita, T.; Ishizawa, Y.; Yagi, N.; Takata, M.; Kitamura, H.; Takahara, A.; Sakurai, K.; Tashiro, K.; Kanaya, T.; Amemiya, Y.; Horie, K.; Takenaka, M.; Jinmai, H.; Okuda, H.; Akiba, I.; Takahashi, I.; Yamamoto, K.; Hikosaka, M.; Sakurai, S.; Shinohara, Y.; Sugihara, Y.; Okada, A. Experimental station for multiscale surface structural analyses of soft-material films at SPring-8 via a GISWAX/GIXD/XR-integrated system. *Polym. J.* **2013**, *45* (1), 109–116.

(19) Cubitt, R.; Fragneto, G. D17: the new reflectometer at the ILL. *Appl. Phys. A: Mater. Sci. Process.* **2002**, *74* (1), s329–s331.

(20) Webster, J. R. P.; Langridge, S.; Dalglish, R. M.; Charlton, T. R. Reflectometry techniques on the Second Target Station at ISIS: Methods and science. *Eur. Phys. J. Plus* **2011**, *126* (111), 112–117.

(21) Mai, S.-M.; Fairclough, J. P. A.; Viras, K.; Gorry, P. A.; Hamley, I. W.; Ryan, A. J.; Booth, C. Chain folding in semicrystalline oxyethylene/oxybutylene diblock copolymers. *Macromolecules* **1997**, *30* (26), 8392–8400.

(22) DOI: 10.5291/ILL-DATA.9-13-407.

(23) Van Krevelen, D. W. *Properties of Polymers*, 4th ed.; Elsevier Science: Amsterdam, 2009.

(24) Nelson, A. Co-refinement of multiple-contrast neutron/X-ray reflectivity data using MOTOFIT. *J. Appl. Crystallogr.* **2006**, *39* (2), 273–276.

(25) <http://octa.jp>.

(26) Hamley, I. H.; Fairclough, J. P. A.; Ryan, A. J.; Bates, F. S.; Towns-Andrews, E. Crystallization of nanoscale-confined diblock copolymer chains. *Polymer* **1996**, *37* (19), 4425–4429.